ADVANCED ENERGY MATERIALS
www.advenergymat.de

Solvent-Dependent Singlet Fission in Diketopyrrolopyrrole Dimers: A Mediating Charge Transfer versus a Trapping Symmetry-Breaking Charge Separation

Ilias Papadopoulos, Maria João Álvaro-Martins, Desiré Molina, Patrick M. McCosker, Paul A. Keller, Timothy Clark, Ángela Sastre-Santos, and Dirk M. Guldi**

Dedicated to Professor Patrik Schmuki on the occasion of his 60th birthday.

Three diketopyrrolopyrrole (DPP) dimers, linked via different dithienylphenylene spacers, *ortho*-DPP (*o*-DPP), *meta*-DPP (*m*-DPP), and *para*-DPP (*p*-DPP), are synthesized, characterized, and probed in light of intramolecular singlet fission (*i*-SF). Importantly, the corresponding DPP reference (DPP-Ref) singlet and triplet excited state energies of 2.22 and 1.04 eV, respectively, suggest that *i*-SF is thermodynamically feasible. The investigations focus on the impact of the relative positioning of the DPPs, and give compelling evidence that solvent polarity and/or spatial overlap govern *i*-SF dynamics and efficiencies. Polar solvents make the involvement of an intermediate charge transfer (CT) state possible, followed by the population of $^1(T_1T_1)$ and subsequently $(T_1 + T_1)$, while spatial overlap drives the mutual interactions between the DPPs. In *o*-DPP, the correct balance between polar solvents and spatial overlap leads to the highest triplet quantum yield (TQY) of 40%. Notable is the superimposition of CT and triplet excited states, preventing an accurate TQY determination. For *m*-DPP, poorer spatial overlap correlates with weaker CT character and manifests in a TQY of 11%. Strong CT character acts as a trap and prevents *i*-SF, as found with *p*-DPP. The DPP separation is decisive, enabling a symmetry-breaking charge-separated state rather than CT formation, shutting down the formation $^1(T_1T_1)$.

1. Introduction

The down-conversion of singlet excited states by means of singlet fission (SF) is currently at the forefront of advanced photon management. SF enables multiple excitons to be generated after the absorption of just a single photon.[1–9] By integrating SF materials into solar-cell architectures, it is feasible to increase the overall efficiency of solar cells by pushing the Shockley–Queisser limit from 32% to approximately 45%. Several requirements must, however, be met to allow for efficient SF well beyond 100%.[10,11]

Thermodynamically, the energy level of the singlet excited state (S_1) must be equal to or higher than twice that of the triplet excited state (T_1); $(S_1) \geq 2(T_1)$.[2,3,12] In addition, the energy levels of higher-lying triplet excited states (T_2) should exceed twice the energy of the lowest-lying triplet excited state; $(T_2) \geq 2(T_1)$.[2,3,12] The latter avoids (T_2) population as a product of triplet–triplet annihilation up-conversion (TTA-UC).[2,3,12] Sufficient electronic interaction between two or more chromophores is essential, and is usually realized for monomers by overlaps in the crystal packing or high concentrations in the solid state or solution, respectively.[12–16] Dimers, in which different spacers are employed to link the chromophores, rather than monomers, represent yet another strategy to adjust and fine-tune, for

I. Papadopoulos, Prof. D. M. Guldi
Department of Chemistry and Pharmacy
Interdisciplinary Center for Molecular Materials (ICMM)
Friedrich-Alexander-Universität Erlangen-Nürnberg (FAU)
Egerlandstr. 3, Erlangen 91058, Germany
E-mail: dirk.guldi@fau.de

The ORCID identification number(s) for the author(s) of this article can be found under https://doi.org/10.1002/aenm.202001496.

DOI: 10.1002/aenm.202001496

M. J. Álvaro-Martins, Dr. D. Molina, Prof. Á. Sastre-Santos
Área de Química Orgánica
Instituto de Bioingeniería
Universidad Miguel Hernández
Avda. de la Universidad s/n
Elche 03203, Spain
E-mail: asastre@umh.es

P. M. McCosker, Prof. T. Clark
Department of Chemistry and Pharmacy
Computer-Chemie-Center (CCC)
Friedrich-Alexander-Universität Erlangen-Nürnberg
Nägelsbachstr. 25, Erlangen 91052, Germany

P. M. McCosker, Prof. P. A. Keller
School of Chemistry and Molecular Bioscience
Molecular Horizons
Illawarra Health and Medical Research Institute
University of Wollongong
Wollongong, NSW 2522, Australia

instance, electronic coupling, spatial overlap, and to probe the SF mechanisms, kinetics, and efficiencies.[5,8]

Currently, not all mechanistic aspects of SF are completely understood.[17,18] Although SF has seemingly many mechanistic facets, two main pathways have emerged. The first one is a one-step, direct mechanism, by which the initial (S_1S_0) transforms into the final $^1(T_1T_1)$ without populating any transient intermediate. The second is the indirect, two-step mechanism, in which the population of the final $^1(T_1T_1)$ is mediated by a transient state, either virtual or real.[12,19–27]

Acenes, in general, and pentacenes in particular, fulfill all SF requirements and, consequently have attracted a great deal of attention.[16,24,28–35] Other promising SF materials include rylene diimides[26,36–44] and diketopyrrolopyrroles (DPPs).[45–51] Incentives for this study were to improve our understanding of intramolecular SF (*i*-SF) in DPP dimers. In general, DPPs are strongly fluorescent, feature high stability, are widely accessible due to their relatively simple synthesis, and exhibit good carrier mobility.[52–58] DPPs are found in a broad range of applications including field-effect transistors, solar-cell devices, fluorescence imaging and importantly, SF.[52,53,58–66] Some SF reports are known from the literature, but most focus on intermolecular SF (inter-SF) in monomers,[45,46,49] rather than intra-SF in dimers.[48,50] As far as the triplet excited state (T_1) energies of DPPs are concerned, they range from 1.02 to 1.21 eV.[45,46,67]

In this study, we have synthesized, characterized, and probed a versatile set of three different DPP dimers, in which the DPPs are linked by dithienylphenylene spacers substituted in the *ortho*-, *meta*-, and *para*-positions; *o*-DPP, *m*-DPP, and *p*-DPP, respectively. Different DPP positions allow the influence of spatial overlap on the SF dynamics and efficiencies to be explored. In addition, the use of different solvents, from non-polar toluene to polar benzonitrile, makes analysis of the participation of a transient CT state and its impact on SF possible.

2. Results and Discussion

2.1. Synthesis

o-DPP, *m*-DPP, and *p*-DPP were obtained by Suzuki–Miyaura coupling between BrDPP[68] and the boronic esters **2**, **3**,[69] and **4**, respectively, in 53%, 43%, and 36% yield, respectively (**Scheme 1**). BrDPP was prepared as previously described from DPP-Ref. [70,71] *p*-DPP was previously synthesized by direct heteroarylation, but not completely characterized.[72] All three dimers are soluble in common organic solvents, such as toluene, dichloromethane (DCM), and chlorobenzene (Figures S31–S53, Supporting Information).

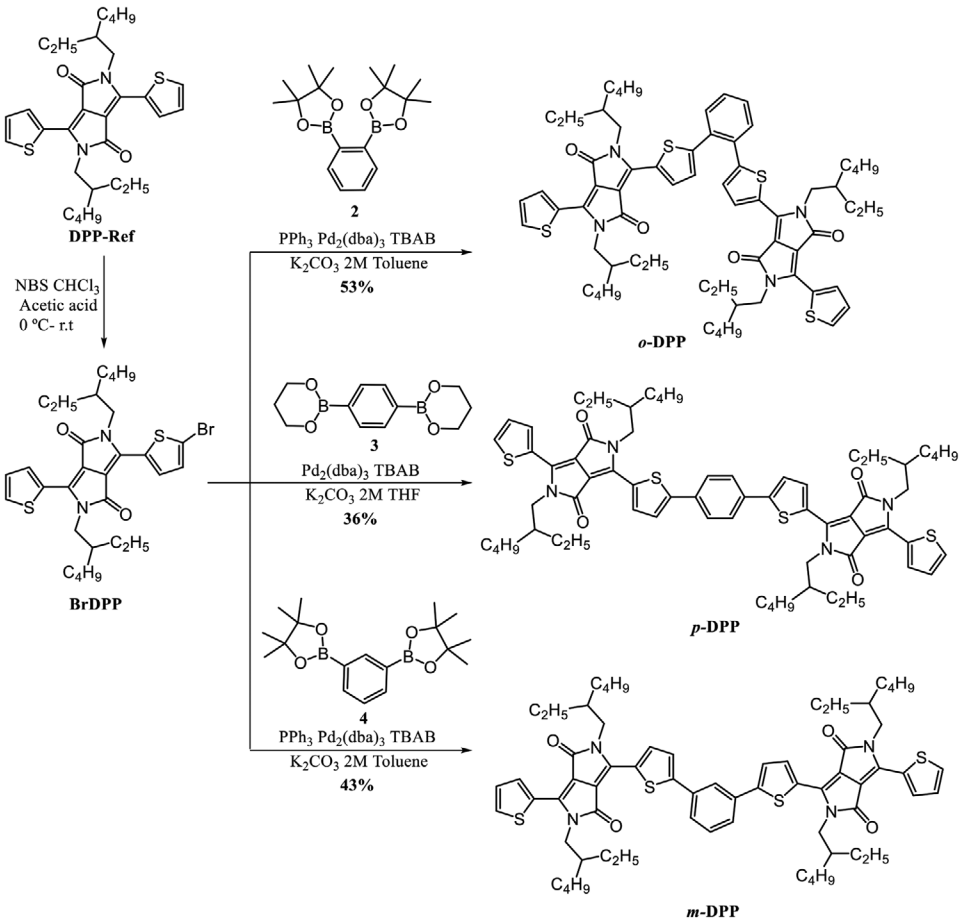

Scheme 1. Synthesis of *o*-DPP, *m*-DPP, and *p*-DPP by Suzuki–Miyaura coupling and chemical structure of DPP-Ref and BrDPP.

2.2. Theory

Density functional theory (DFT) and its time-dependent (TD-DFT) counterpart were used to investigate the ground (S_0) and excited state (S_1, T_1, T_2) properties of DPP-Ref, *o*-DPP, *m*-DPP, and *p*-DPP. The S_0 geometries were found using the B3LYP hybrid functional with Grimme's dispersion correction (D3) and Becke–Johnson dampening (BJ),[73–76] combined with the 6–311G(d) basis set for the DPP-Ref structure, or the split valence 6–31G(d) for the dimers.[77,78] It was found that substitution of the nitrogen atoms with at least isobutyl groups was necessary to reproduce the geometry and vertical excitations (VE) of DPP-Ref. The dimers were therefore optimized with isobutyl substituents (Figure S29 and Table S3, Supporting Information).

Comparison of different conformations of DPP-Ref indicated the thiophene-*trans* configuration to be lowest in energy, as also found for the dimer conformers (Figure S30, Supporting Information). Subsequent analysis of the *o*-DPP conformers revealed that stacking of the DPP monomers resulted in the lowest energy structure, whereas *m*-DPP and *p*-DPP preferred monomer separation (**Figure 1**). The separation of monomer planes in *o*-DPP was found to be 5.7 Å and in contrast, the *m*-DPP and *p*-DPP dimers are significantly separated such that spatial overlap is minimized or completely eliminated respectively.

An approximation of the SF thermodynamics of the DPP dimers was obtained by calculating TD-DFT VE (S_1, T_1, T_2) at the M06-2X/def2-TZVP level of theory (Table S5, Supporting Information). The S_0–S_1 vertical excitations were found to be in the order of 2.61–2.27 eV, and tended toward lower energies in the order DPP-Ref > *o*-DPP > *m*-DPP > *p*-DPP, in agreement with the steady-state absorption—vide infra. Subsequently, the SF process was predicted to be exothermic for all dimers, with S_1/T_1 (VE) ratios of 2.34, 2.40, and 2.38 for *o*-DPP, *m*-DPP, and *p*-DPP, respectively. In contrast, the TTA-UC process was found to be endothermic, with T_2/T_1 ratios of 2.52, 2.50, and 2.44, respectively, in turn ruling out the presence of delayed fluorescence. Both S_1/T_1 and T_2/T_1 for all dimers were found to be of a similar value, and should therefore not impact on the SF dynamics of the dimers differently.

The charge transfer/resonance character of SF dimers has recently been highlighted to enhance the formation of the correlated triplet pair significantly.[79] Studying the spin distribution in DPP-linked pentacene dimers revealed that strong charge transfer/resonance character of the S_1 state correlated with $^1(T_1T_1)$ exciton formation and subsequent triplet quantum yields (TQY). The DPP dimers investigated were found to have stable ground-state wavefunctions, namely, non-biradicals with satisfactory closed-shell description of the singlets. Subsequent analysis of the TD-DFT S_0–S_1 VE in all dimers indicated S_1 to be a linear combination of the frontier molecular orbitals (FMOs) ± 1 (Figures S37–S40, Supporting Information).

The FMOs in all dimers were delocalized over both DPPs and only subtle differences were noted. Briefly, the *o*-DPP highest occupied molecular orbitals (HOMOs) and lowest occupied molecular orbitals (LUMOs) were equally and unequally distributed across the subunits, respectively, with minimal delocalization onto the benzene linker. In contrast, *m*-DPP and *p*-DPP FMOs were equally distributed and included the orbitals of the benzene linker. In addition, analysis of the FMO's contributions to the TD-DFT S_0–S_1 VE indicated minimal redistribution of electron density, even in the case of *o*-DPP, where the multiple contributions were almost equally distributed, minimizing the electron density localization. As a result, the S_0–S_1 VE can primarily be described as π–π^* in character, with a minimal degree of charge transfer/resonance, and should hinder the $^1(T_1T_1)$ exciton formation, resulting in the low TQYs observed—vide infra.

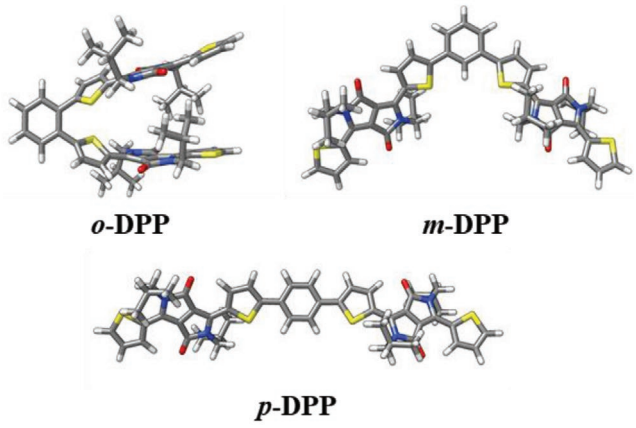

Figure 1. Optimized structures of *o*-DPP, *m*-DPP, and *p*-DPP.

2.3. Photophysical Characterization

2.3.1. Steady-State Characterization

Steady-state absorption measurements were performed to explore the ground state of the DPPs. Measurements were conducted in solvents of different polarity, that is, toluene and benzonitrile, to investigate the influence of polarity on the SF-mechanism and its dynamics. The DPP-Ref absorptions in toluene included a set of well-resolved maxima between 400 and 600 nm, which represent the 0–*0 and 0–*1 transitions to the lowest singlet excited states. In addition, maxima were seen between 300 and 400 nm, representing the corresponding transitions to higher singlet excited states. Extinction coefficients as high as 30 000 M^{-1} cm^{-1} were found in toluene. Changing the solvent to benzonitrile led to no significant differences.

Analysis of *o*-DPP, *m*-DPP, and *p*-DPP revealed significant differences between them. Notably, in DPP-Ref the intensities of the 0–*0 to 0–*1 transitions decreased, while in *o*-DPP they were reminiscent of the absorption pattern of *H*-aggregates, that is, of equal intensity, suggesting sizeable interactions between the DPPs. Other differences included a red-shift of about 20 nm and an increase of the extinction coefficient to about 65 000 M^{-1} cm^{-1}. *m*-DPP features are much closer to those of DPP-Ref, despite the observation of a 30 nm red-shift and an extinction coefficient of nearly 93 000 M^{-1} cm^{-1}. Lastly, *p*-DPP exhibits broad and featureless absorption peaks, which are roughly 60 nm red-shifted compared to DPP-Ref with extinction coefficients as large as 96 000 M^{-1} cm^{-1}. Overall, the steady-state absorption measurements (**Figure 2**a) reveal increasing red-shifts and extinction coefficients in the order

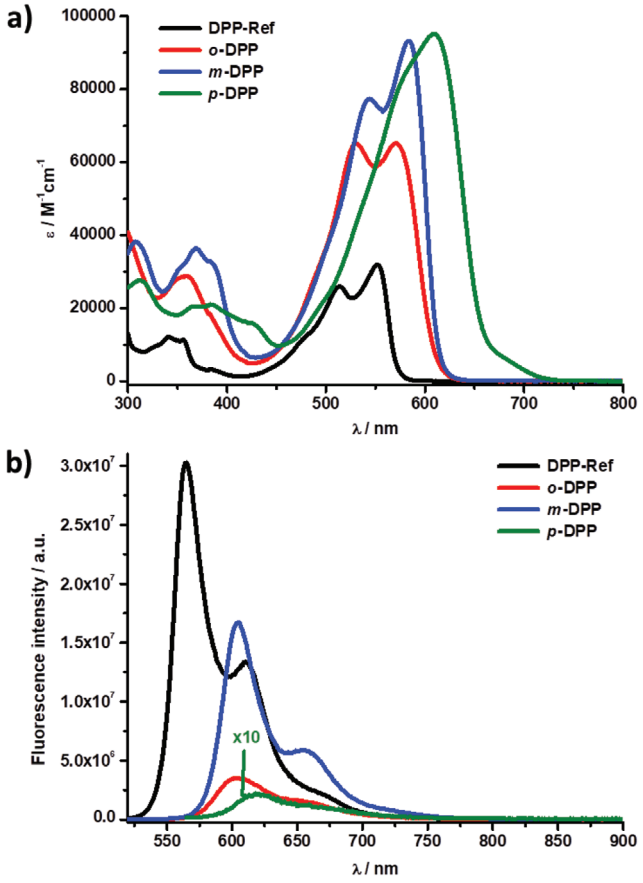

Figure 2. a) Room-temperature absorption spectra of DPP-Ref (black), *o*-DPP (red), *m*-DPP (blue), and *p*-DPP (green) in toluene. b) Respective fluorescence spectra in toluene following photoexcitation at 545 nm for *o*-DPP and *m*-DPP, 550 nm for *p*-DPP, and 505 nm for DPP-Ref with optical densities of 0.025.

o-DPP < *m*-DPP < *p*-DPP. It is safe to postulate that the electronic couplings, which differ in the DPP dimers, are sufficient to govern *i*-SF—vide infra.[80]

Steady-state fluorescence measurements provided first indications of differences in the excited states. For DPP-Ref, the fluorescence maximum lies between 500 and 750 nm and the fluorescence quantum yield (FQY) between 69.5% in toluene and 66.7% in benzonitrile. Common to *o*-DPP, *m*-DPP, and *p*-DPP are hypsochromic shifts, which coalesced with the corresponding shifts seen in the absorption measurements (Figure 2b), and significant FQY quenching. Starting with *m*-DPP, a 46.6% FQY suggested moderate inter-DPP interactions. *o*-DPP is subject to a much stronger fluorescence quenching with an FQY of 12.1% and the strongest quenching is found for *p*-DPP with a 1.4% FQY. In contrast to DPP-Ref, changing the solvent from toluene to benzonitrile resulted in further FQY quenching: 5.3% (*m*-DPP), 2.1% (*o*-DPP), 1.2% (*p*-DPP) (Figure S1 and Table S1, Supporting Information).

The steady-state absorption and fluorescence measurements indicated that for *o*-DPP, the intensity increase of the 0–*1 absorption is accompanied by a quenched FQY, when compared to DPP-Ref. Such trends are in line with intramolecular forces between slightly displaced, parallel arranged DPPs, as in *H*-type aggregates. Concentration independence underlines the intra- rather than inter-molecular nature of the DPP interactions in *o*-DPP. The solvent-dependent FQYs suggest an excited-state deactivation involving the formation of either charge transfer (CT) state, relating to the partial transfer of electron density, or symmetry-breaking charge-separated (SBCS) state, relating to the full transfer of electron density and, in turn, the full separation of electrons and holes. Involvement of a CT/SBCS state induces red-shifts in the *H*-type aggregates, which usually feature blue-shifts.[81–83] Similarly, a deactivation via a CT state and/or a SBCS state in *H*-aggregates was reported for the case, in which a xanthene bridge was used in DPP dimers.[50] For *p*-DPP, the broadened absorption goes hand-in-hand with the most strongly quenched fluorescence among the DPP dimers. Again, the quenched and, more importantly, the solvent-dependent, albeit weak, FQYs suggest the involvement of either CT state or SBCS state. The broadening of the absorption features is attributed to the free and unhindered rotation of the DPPs, due to the minimal steric interaction of the *para*-position, which was supported by theory. Finally, for *m*-DPP both absorption and fluorescence resemble what is seen for the reference. The overall strength of the interaction is expected to be the weakest among the DPP dimers, as the phenyl linker affords better electronic communication in case of *ortho*- and *para*-substitutions.[84,85]

In low-temperature measurements with DPP-Ref at 80 K in 2-methyltetrahydrofuran (MeTHF) and in the presence of ethyliodide (EtI) to enhance the triplet formation, a 1185 nm feature was ascribed to phosphorescence. Correspondingly, a triplet excited state (T_1) energy of 1.04 eV was derived—Figure S2, Supporting Information. Comparing a T_1 energy of 1.04 eV with S_1 energies as high as 2.22 eV in DPP-Ref and as low as 2.08 eV in *m*-DPP renders *i*-SF thermodynamically feasible.

2.3.2. Electrochemical and Spectroelectrochemical Characterization

Electrochemical properties of the three dimers were examined by cyclic voltammetry (CV) using CH_2Cl_2 as solvent containing 0.1 M tetrabutylammonium hexafluorophosphate ($TBAPF_6$) as supporting electrolyte (**Figure 3**, **Table 1**). The three dimers present a similar band gap owing to the fact that the electron donor and the acceptor fragments are the same. However, *p*-DPP presents the lowest E_g^{cv} among the three different dimers. Based on a push–pull structure, the LUMO energy level is controlled by the electron accepting (deficient) unit, while the HOMO energy level is governed by the electron rich (donating) unit. DPP-Ref has the largest band gap with a value of 2.2 eV when compared to the DPP dimers, which are between 2.0 and 2.1 eV.

Spectroelectrochemical (SEC) measurements were conducted to register the optical features of both the one-electron reduced and oxidized forms of the DPP dimers and to use them to interpret the time-resolved transient absorption measurements. Experiments were conducted in a toluene/acetonitrile mixture (4/1 v/v) with 0.1 M $TBAPF_6$ as supporting electrolyte. In the case of *o*-DPP, applying +1.0 V resulted in fully reversible spectroscopic features of its one-electron oxidized form in the 650–1000 nm range with maxima at 780 and 900 nm (**Figure 4**a). In contrast, a potential of −1.5 V resulted

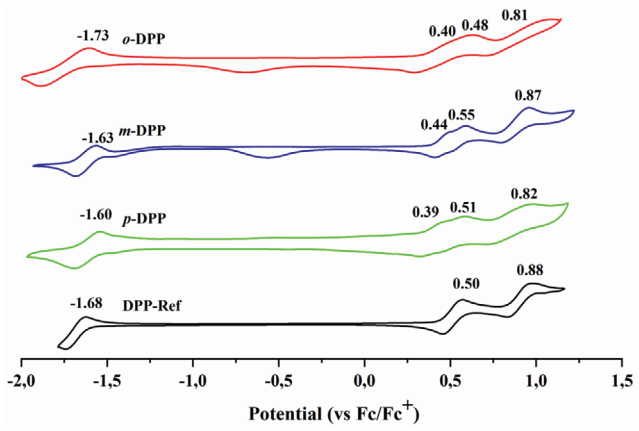

Figure 3. Cyclic voltammograms of *o*-DPP, *m*-DPP, *p*-DPP, and DPP-Ref in CH_2Cl_2 containing 0.1 M $TBAPF_6$ as supporting electrolyte and measured against Fc/Fc^+.

in the formation of its semi-stable one-electron reduced form with only a single maximum at approximately 480 nm. Unfortunately, the ground-state absorption superimposes the feature of the one-electron reduced form, which, in turn, could not be fully resolved (Figure 4b). Similar results were gathered for *m*-DPP and *p*-DPP (Figures S4 and S5, Supporting Information).

2.3.3. Time-Resolved Characterization

Time-correlated single photon counting (TCSPC) measurements, with a 530 nm excitation wavelength, revealed for DPP-Ref a single fluorescent component with a lifetime of 5.5 ns in toluene. *o*-DPP, *m*-DPP, *p*-DPP gave rise to two fluorescent components, a short-lived one on the picosecond timescale and a long-lived one on the nanosecond timescale.[86] In detail, the lifetimes in toluene are 832 ps and 2.4 ns for *o*-DPP, 490 ps and 3.6 ns for *m*-DPP, and <200 ps and 2.5 ns for *p*-DPP. A change to benzonitrile only affected the short-lived component without, however, impacting the long-lived one (Figure S6, Supporting Information). A summary is given in **Table 2**.

Subsequently, time-resolved transient absorption spectroscopy on the femto- (fsTAS) and nanosecond (nsTAS) timescales were performed following 530 nm excitation. Lifetimes

Table 1. Optical and electrochemical parameters of *o*-DPP, *m*-DPP, *p*-DPP, and DPP-Ref.

Compound	E_{red1} [eV]	E_{oxi1} [eV]	$E_{g,opt}$[a)]/E_{EC}[b)] [eV]	HOMO[c)]	LUMO[d)]
p-DPP	−1.60	0.39	2.02/1.99	−5.19	−3.20
m-DPP	−1.63	0.44	2.09/2.07	−5.24	−3.17
o-DPP	−1.73	0.40	2.11/2.03	−5.20	−3.17
DPP-Ref	−1.68	0.50	2.23/2.18	−5.30	−3.12

The energy positions of the HOMOs were estimated from the onset values for the oxidation potentials through the equation.
[a)]$E_{g,opt}$ (eV) was determined from the intersection of normalized absorption and emission spectra registered in CH_2Cl_2; [b)]$E_{g,EC} = E_{red1} - E_{oxi1}$; [c)]HOMO = $-|E_{ox1}$(vs Fc/Fc^+) + 4.8|; [d)]The LUMO values were calculated by LUMO = HOMO + $E_{g,EC}$ (eV).

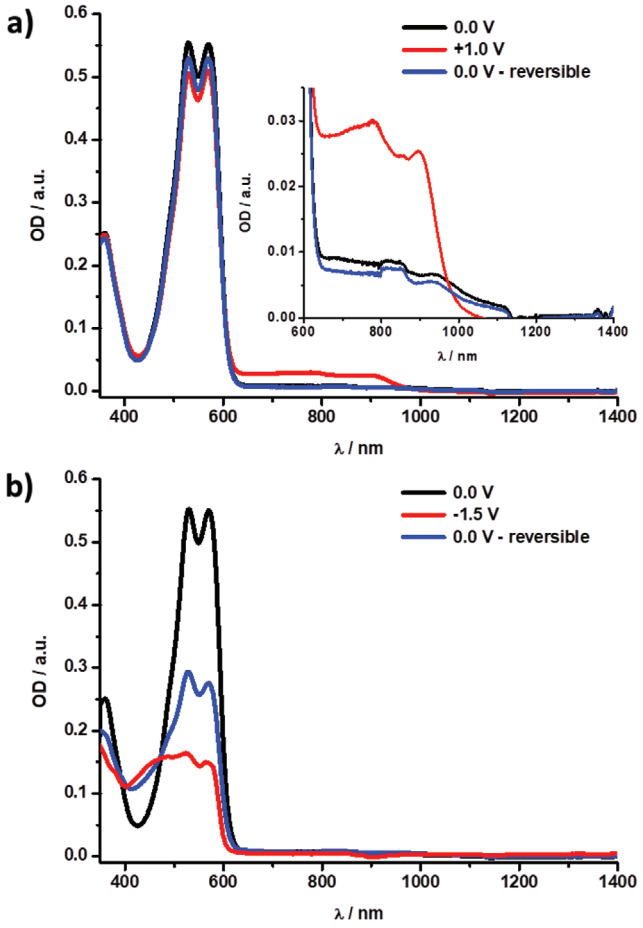

Figure 4. Spectroelectrochemical features of the a) one-electron oxidized and b) one-electron reduced forms of *o*-DPP in a toluene/acetonitrile solution (4/1 v/v) with 0.1 M $TBAPF_6$ as supporting electrolyte. Similar results were gathered for *m*-DPP and *p*-DPP (Figures S4 and S5, Supporting Information).

were obtained by means of GloTarAn target analyses. In DPP-Ref, excitation is immediately followed by the formation of the singlet excited state (S_1). In toluene, maxima are found at 435, 710, and 885 nm, while minima evolved at 513, 562, and 616 nm (Figure S8a,c, Supporting Information). The former minima relate to ground-state bleaching (GSB) and the latter to stimulated emission (SE). All of these features were replaced within 4.5 ps (Figure S8b,d, Supporting Information) by an intermediate state, which was characterized by subtle shifts of the 885 nm maximum and the 562 and 616 nm minima. The underlying process corresponds to solvent reorganization, which was due to increasing the solvation energy of the excited state leading to $(S_1)_{Sol}$.[29,87] From $(S_1)_{Sol}$, the complete reinstatement of the ground state (S_0) is reached within 6.0 ns (Figure S10, Supporting Information). Similar results were gathered for DPP-Ref in benzonitrile (Figures S9 and S11, Supporting Information).

An initial analysis of *o*-DPP, *m*-DPP, and *p*-DPP showed that all of them featured in toluene the same initial singlet excited state (S_1S_0) with lifetimes of 9.9, 7.8, and 15.5 ps, respectively. Common to all (S_1S_0) was the solvent reorganization to afford

Table 2. Lifetimes obtained from GloTarAn target analysis of the time-resolved fluorescence (TCSPC) and transient absorption measurements, together with the calculated triplet quantum yields (TQY) in toluene and benzonitrile.

Sol	Compound	$\tau(S_1S_0)$ [ps]	$\tau(S_1S_0)_{Sol}$ [ps]	$\tau(S_1S_0)_{Sol}$/τ(SBCS) [ns]	$\tau^1(T_1T_1)$ [ns]	$\tau(T_1 + T_1)$ [µs]	TQY [%]	τ_{TCSPC}	
								[ps]	[ns]
Tol	DPP-Ref	4.5	6.0 ns	—	—	—	—	—	5.5
	o-DPP	9.9	576	2.3	—	—	—	832	2.4
	m-DPP	7.8	372	3.7	—	—	—	490	3.6
	p-DPP	15.5	77.0	1.8	—	—	—	<200	2.5
BN	DPP-Ref	8.0	6.4 ns	—	—	—	—	—	5.9
	o-DPP	33.7	313	3.9	42.0	15.0	40	389	3.9
	m-DPP	14.0	298	4.4	86.5	98.9	11	298	3.8
	p-DPP	18.2	56.8	2.2	—	—	—	<200	2.5

$(S_1S_0)_{Sol}$. The underlying lifetimes of 576 ps (*o*-DPP), 372 ps (*m*-DPP), and 77 ps (*p*-DPP) were, however, shorter than what was seen for DPP-Ref. It was also noted that the lifetimes reflected the strength of intramolecular DPP interactions. In stark contrast to the conclusions drawn for DPP-Ref, *o*-DPP, *m*-DPP, and *p*-DPP populate yet another, third state, whose lifetimes are 2.3, 3.7, and 1.8 ns, respectively, and lead to the quantitative ground-state recovery. Interesting is the fact that the third species bears similarities with the aforementioned $(S_1S_0)_{Sol}$ signatures. In other words, it has still some singlet excited state character. Next to the $(S_1S_0)_{Sol}$ signatures, transients at 460, 650, and 1000 nm resemble the fingerprints seen in SEC (Figure 4 and Figures S4 and S5, Supporting Information). We postulate in line with recent work mixing of the singlet excited state with a CT state and defining the third species as $(S_1S_0)_{CT}$.[25,29,88] Noteworthy, the lifetimes of $(S_1S_0)_{Sol}$ and $(S_1S_0)_{CT}$ match those of the short- and long-lived fluorescent components detected in the TCSPC measurements – *vide supra* (Table 2). The only notable differences between *o*-DPP, *m*-DPP, and *p*-DPP are the expected shifts in the GSB and SE features. Importantly, no appreciable population of any triplet excited state is observed in toluene (Figures S12–S15, S18,S19, Supporting Information).

The strong impact of solvent polarity changes on the FQYs suggested a subtle interplay between the different states in the excited state deactivation of *o*-DPP, *m*-DPP, and *p*-DPP. A comparison with toluene corroborates that the first, second, and third species are still involved in the excited-state deactivation. The longer (S_1S_0) lifetimes in benzonitrile are due to the higher viscosity, which slows down solvent reorganization.

Analysis of the results for *o*-DPP showed that, after solvent reorganization $(S_1S_0)_{Sol}$, a stronger CT contribution in $(S_1S_0)_{CT}$ is derived from the positive transient at 650 nm (**Figure 5**a,c). Likewise, a shorter $(S_1S_0)_{CT}$ lifetime relative to toluene stems from the CT-stabilization in more polar solvents. $(S_1S_0)_{CT}$ also experienced a stronger CT-mixing, which is manifested in an intense peak at 480 nm and depletion of GSB. Both characteristics are in line with the SEC features seen for the one-electron reduced form of *o*-DPP (Figure 4b). Lifetimes of $(S_1S_0)_{Sol}$ and $(S_1S_0)_{CT}$ (Figure 5b,d and Table 2) match the corresponding TCSPC lifetimes in benzonitrile (Table 2)—vide supra. Contrary to the results in toluene, the $(S_1S_0)_{CT}$ deactivation is linked to the population of two additional states. Of great importance is the fact that none of these two additional states resemble the CT character seen, for example, in $(S_1S_0)_{CT}$, or the $(S_1S_0)_{Sol}$ features. In particular, maxima are found at 470 (broad) and 555 nm, which are complemented by minimum at 585 nm. Of equal importance is the fact that they are spectrally nearly identical.

To clarify the nature of these two additional states, we turned to triplet–triplet sensitization measurements with *N*-methylfulleropyrrolidine (*N*-MFP, Figure S23, Supporting Information) as a triplet–triplet energy transfer (TTET) donor and *o*-DPP as TTET acceptor. Photoexcitation was performed at 430 nm. In the case of *o*-DPP, again maxima at 470 (broad) and 555 nm and a minimum at 585 nm were seen to grow in at the expense of the triplet excited state maximum of *N*-MFP at 700 nm. The correspondingly formed (T_1S_0) decays with approximately 20 µs to the ground state. Considering the appreciable resemblance between the (T_1S_0) signature in TTET and the spectroscopic signature of the first of the two additional states, we infer the population of $^1(T_1T_1)$ in *o*-DPP, that is, two triplet excited states are formed (**Figure 6**a,c). The re-intensification of the GSB was emphasized in Figure S22, Supporting Information. In contrast to the approximately 20 µs lifetime of (T_1S_0), $^1(T_1T_1)$ is short lived. It is within 42.0 ns that $^1(T_1T_1)$ transforms in the second of the two additional states.[89] We rationalize the transformation to the decoherence of $^1(T_1T_1)$ (Figure 6b,d and Table 2) and the formation of the uncorrelated triplet excited state $(T_1 + T_1)$ (Figure 6a,c). The lifetime of the latter is 15.0 µs and agrees well with that derived for (T_1S_0) (Figure 6b,d and Table 2). In short, the existence of these two triplet-based species, inferred by a reasonable coupling of the thiophene–phenyl–thiophene bridges due to rotational freedom/heteroatom effect, corroborated *i*-SF, as conventional ISC would lead to only one triplet excited state. Despite the lack of CT character in $^1(T_1T_1)$ and $(T_1 + T_1)$, an alternative deactivation route should be mentioned: two subsequently formed CTs with singlet and triplet spin, respectively.

The TQY was calculated using the method, which incorporates the singlet (ε_{S1*}) and triplet (ε_{T1*}) excited state molar extinction coefficients. As such, a value of 40% was derived (Figure S28a and Table S2, Supporting Information).[28,29,31] Note that the spectroscopic features stemming from the one-electron reduced form superimpose those of $^1(T_1T_1)$ and $(T_1 + T_1)$ making an accurate calculation of the TQYs difficult.

m-DPP acts like *o*-DPP with a biphasic decay of $(S_1S_0)_{CT}$ via $^1(T_1T_1)$ and $(T_1 + T_1)$, but with a shorter $(S_1S_0)_{Sol}$ lifetime of

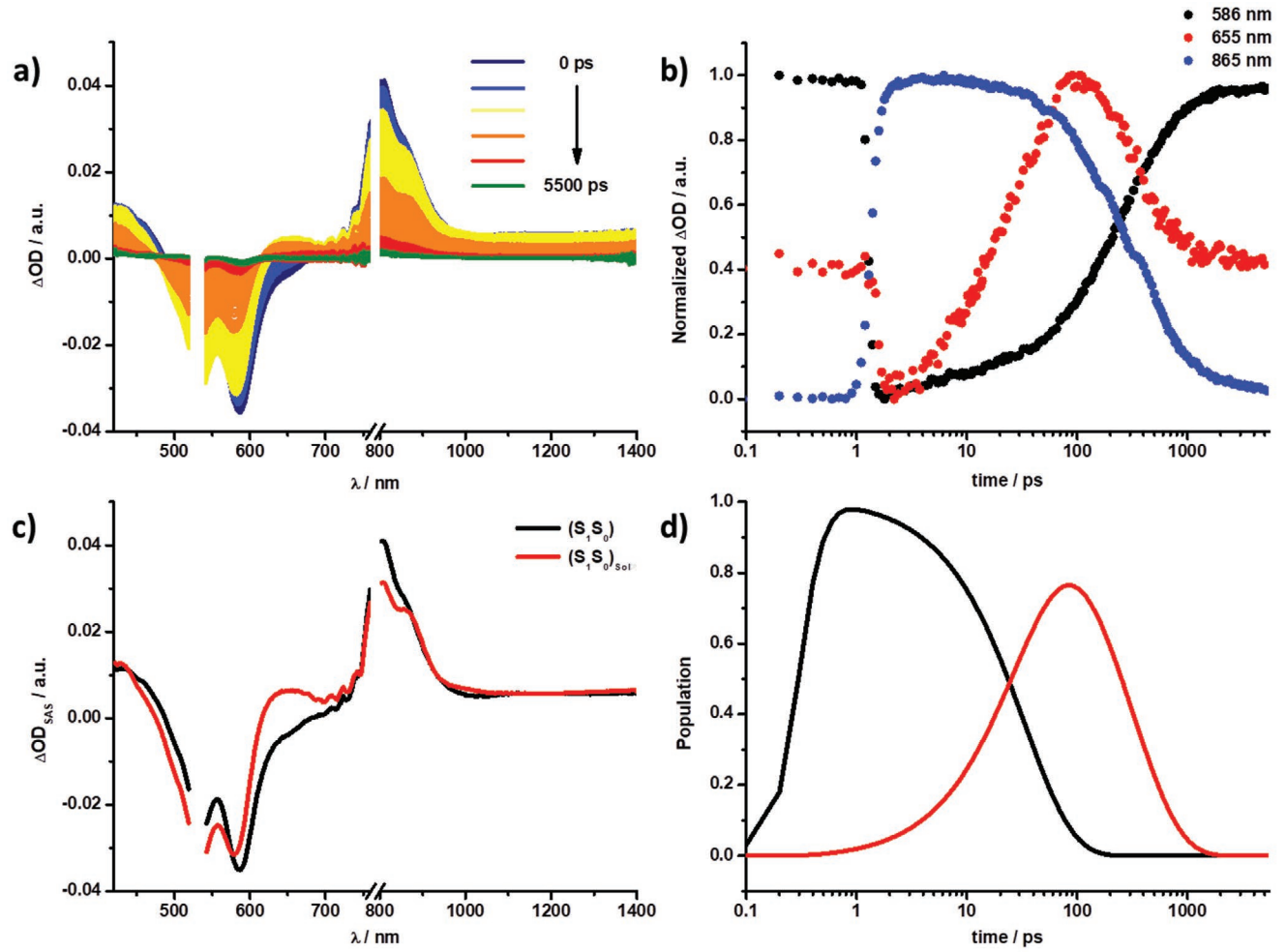

Figure 5. a) Differential femtosecond transient absorption spectra (λ_{ex} = 530 nm, 400 nJ) of *o*-DPP in benzonitrile with time delays between 0 and 5500 ps, following the indicated color gradient. b) Respective time absorption profiles at 586, 655, and 865. c) Deconvoluted femtosecond transient absorption spectra of the singlet excited state (S_1S_0) (black) and intermediate state $(S_1S_0)_{Sol}$ (red) of *o*-DPP in benzonitrile as obtained by target analysis, using the kinetic model shown in Figure 7. d) Respective population kinetics. Note that the subsequent species is omitted as a complete deconvolution failed on this time scale.

298 ps (Figures S16a,c and S17a,c, Supporting Information and Table 2). Overall, the CT character in *m*-DPP is weaker than in *o*-DPP and the TQY is 11%. A likely rationale implies that the inter-DPP electronic coupling is weaker in *m*-DPP across the *meta*-position of the phenyl linker than across the *ortho*-position in *o*-DPP and, in turn, reduces TQY.[84,85]

Finally, for *p*-DPP the shortest $(S_1S_0)_{Sol}$ lifetime and subsequent population of $(S_1S_0)_{CT}$ was observed. Despite this finding, no evidence for any significant triplet excited-state population was gathered. At first glance, $(S_1S_0)_{CT}$ revealed an even stronger CT character for *p*-DPP than for *o*-DPP. A closer look reveals, however, that the feature of the one-electron reduced form covers the range from 400 to 650 nm and, in turn, masks the GSB at around 600 nm (Figures S20a,c and S21a,c, Supporting Information and Table 2). From the strong resemblance of the transient with the SEC fingerprint and the low FQYs in the steady-state assays, a SBCS rather than $(S_1S_0)_{CT}$ formation with a significant CT character is inferred.[50] Minimizing the spatial overlap in *o*-DPP, *m*-DPP, and *p*-DPP enables SBCS. SBCS is, however, detrimental to SF. Therefore, the *i*-SF efficiency follows the trend of *o*-DPP > *m*-DPP >>> *p*-DPP and a schematic diagram of the kinetic models is shown in **Figure 7**.

3. Conclusion

A novel set of three different dimers of DPPs, linked via dithienylphenylene spacers (*o*-DPP, *m*-DPP, and *p*-DPP) was synthesized, characterized, and examined in light of intramolecular singlet fission (*i*-SF). Steady-state absorption and fluorescence measurements indicated the involvement of a charge transfer (CT) and/or SBCS state as part of the SF cascade. Solvent polarity plays the most important role in either CT or SBCS state population. Time-resolved transient absorption spectroscopy revealed two limiting scenarios. On the one hand, CT mediated *i*-SF. Here, non-polar solvents such as toluene were found to be detrimental to the population of any

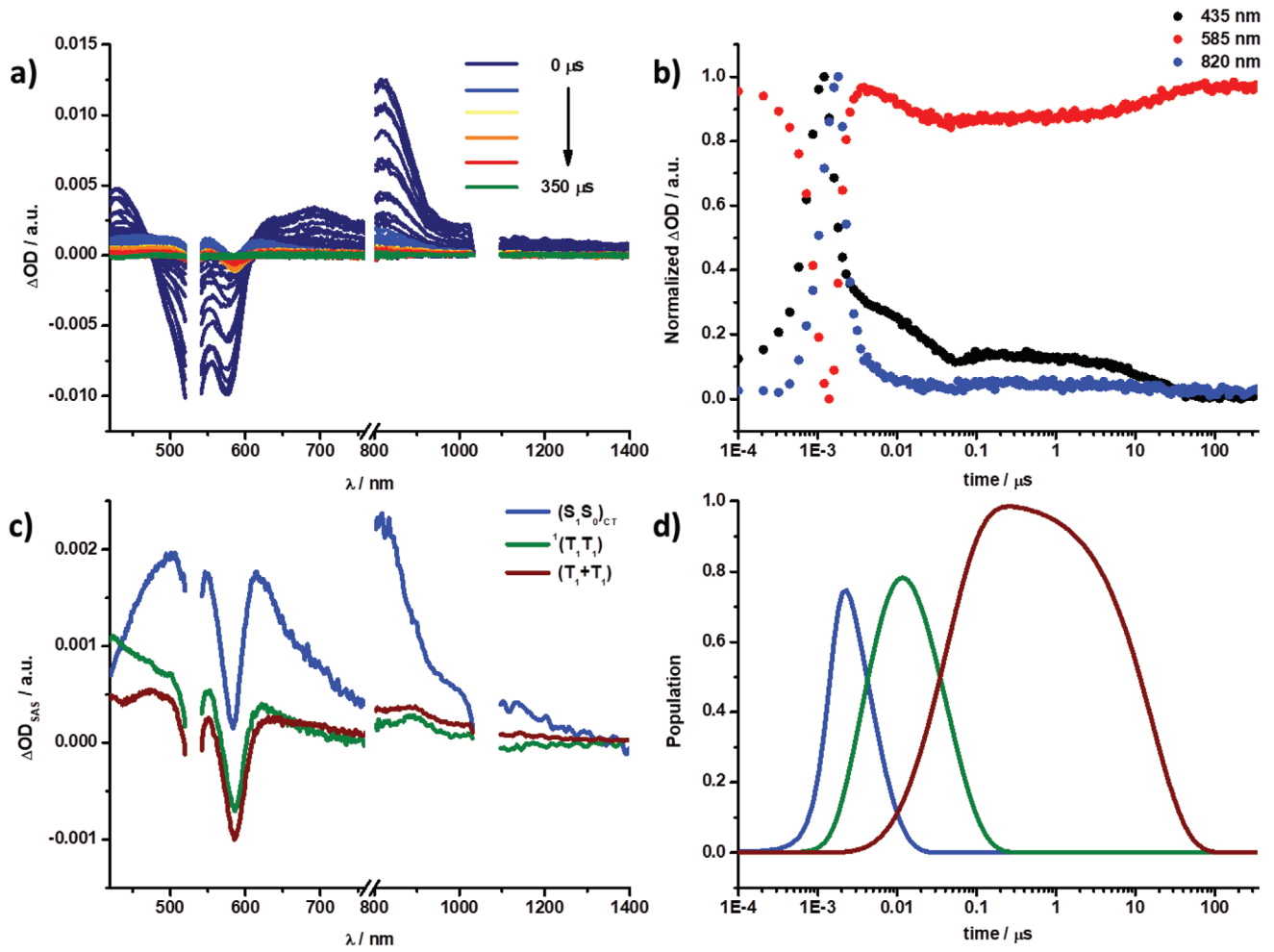

Figure 6. a) Differential nanosecond transient absorption spectra (λ_{ex} = 530 nm, 400 nJ) of *o*-DPP in benzonitrile with time delays between 0 and 350 µs, following the indicated color gradient. b) Respective time absorption profiles at 435, 585, and 820 nm. c) Deconvoluted nanosecond transient absorption spectra of the intermediate singlet excited state with CT character $(S_1S_0)_{CT}$ (blue), correlated triplet excited state $^1(T_1T_1)$ (green), and uncorrelated triplet excited state $(T_1 + T_1)$ (brown) of *o*-DPP in benzonitrile as obtained by target analysis, using the kinetic model shown in Figure 7. d) Respective population kinetics. Note that the intermediate $(S_1S_0)_{Sol}$, which was seen in femtosecond transient absorption, is omitted as the complete deconvolution failed on this time scale.

triplet excited states. It is only polar solvents such as benzonitrile, which enabled the population of $^1(T_1T_1)$ and subsequent

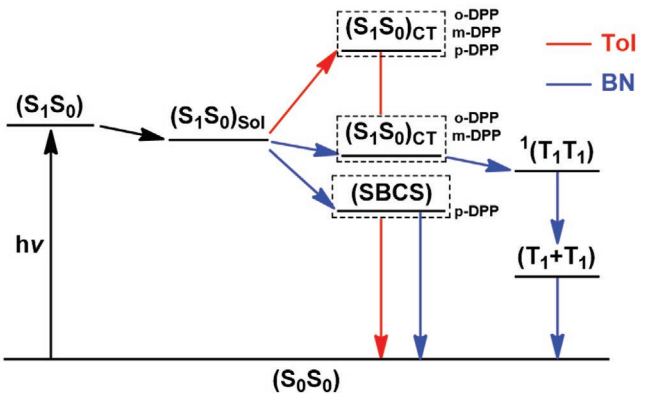

Figure 7. Kinetic models used to fit the transient absorption data of *o*-DPP, *m*-DPP, and *p*-DPP in toluene (red) and benzonitrile (blue).

$(T_1 + T_1)$. On the other hand, the spatial arrangement of the DPPs was important to govern *i*-SF. *o*-DPP had the highest *i*-SF efficiency with a TQY of 40% in benzonitrile. The TQYs were as low as 11% for *m*-DPP and 0% for *p*-DPP when benzonitrile was used as a solvent. As such, with the electronic coupling between the two DPPs, in the case of *o*-DPP, it is sufficiently strong to promote *i*-SF and, at the same time, weak enough to ensure $^1(T_1T_1)$ decoherence and avoid quantitative triplet–triplet annihilation. An alternative mechanism, which is based on the unlikely transient population of two subsequent CT states, namely of singlet and triplet spin ^{1}CT and ^{3}CT, respectively, before just one T_1 is formed, cannot entirely be ruled out. The *i*-SF was quantitatively suppressed in *p*-DPP, where the lack of spatial overlap resulted in a SBCS and shut down the population of $^1(T_1T_1)$ and $(T_1 + T_1)$. Therefore, this study has highlighted that the strength of the CT character, controlled by the solvent polarity, is decisive in balancing the electronic coupling and determining whether it mediates *i*-SF in DPP dimers or blocks *i*-SF due to trapping.

Supporting Information

Supporting Information is available from the Wiley Online Library or from the author.

Acknowledgements

I.P. and M.J.A.-M. contributed equally to this work Á.S.-S. thanks the Ministerio de Economía, Industria y Competitividad of Spain and FEDER funds for financial support (CTQ2017-87102-R). M.J.A.-M. thanks "Beca Santiago Grisolia GRISOLIAP/2017/153" Comunidad Valenciana. D.M. thanks the European Union through the "Programa Operativo del Fondo Social Europeo (FSE) de la Comunitat Valenciana 2014–2020." This work was supported by the Solar technologies go Hybrid (SolTech) initiative of the Bavarian State Government.

Open access funding enabled and organized by Projekt DEAL.

Conflict of Interest

The authors declare no conflict of interest.

Keywords

charge transfer states, diketopyrrolopyrrole dimers, intramolecular singlet fission

Received: May 1, 2020
Revised: September 7, 2020
Published online: October 2, 2020

[1] M. B. Smith, J. Michl, *Chem. Rev.* **2010**, *110*, 6891.
[2] M. B. Smith, J. Michl, *Annu. Rev. Phys. Chem.* **2013**, *64*, 361.
[3] K. Miyata, F. S. Conrad-Burton, F. L. Geyer, X.-Y. Zhu, *Chem. Rev.* **2019**, *119*, 4261.
[4] D. Casanova, *Chem. Rev.* **2018**, *118*, 7164.
[5] B. S. Basel, I. Papadopoulos, D. Thiel, R. Casillas, J. Zirzlmeier, T. Clark, D. M. M. Guldi, R. R. R. Tykwinski, *Trends Chem.* **2019**, *1*, 11.
[6] S. Ito, T. Nagami, M. Nakano, *J. Photochem. Photobiol., C* **2018**, *34*, 85.
[7] N. Monahan, X.-Y. Zhu, *Annu. Rev. Phys. Chem.* **2015**, *66*, 601.
[8] C. Hetzer, D. M. Guldi, R. R. Tykwinski, *Chem. – Eur. J.* **2018**, *24*, 8245.
[9] M. Tuan Trinh, A. Pinkard, A. B. Pun, S. N. Sanders, E. Kumarasamy, M. Y. Sfeir, L. M. Campos, X. Roy, X. Y. Zhu, *Sci. Adv.* **2017**, *3*, e1700241.
[10] W. Shockley, H. J. Queisser, *J. Appl. Phys.* **1961**, *32*, 510.
[11] M. C. Hanna, A. J. Nozik, *J. Appl. Phys.* **2006**, *100*, 074510.
[12] S. R. Yost, J. Lee, M. W. B. Wilson, T. Wu, D. P. McMahon, R. R. Parkhurst, N. J. Thompson, D. N. Congreve, A. Rao, K. Johnson, M. Y. Sfeir, M. G. Bawendi, T. M. Swager, R. H. Friend, M. A. Baldo, T. V. Voorhis, *Nat. Chem.* **2014**, *6*, 492.
[13] J. C. Johnson, T. H. Reilly, A. C. Kanarr, J. van de Lagemaat, *J. Phys. Chem. C* **2009**, *113*, 6871.
[14] H. Marciniak, I. Pugliesi, B. Nickel, S. Lochbrunner, *Phys. Rev. B: Condens. Matter Mater. Phys.* **2009**, *79*, 235318.
[15] M. W. B. Wilson, A. Rao, J. Clark, R. S. S. Kumar, D. Brida, G. Cerullo, R. H. Friend, *J. Am. Chem. Soc.* **2011**, *133*, 11830.
[16] B. J. Walker, A. J. Musser, D. Beljonne, R. H. Friend, *Nat. Chem.* **2013**, *5*, 1019.
[17] P. M. Zimmerman, C. B. Musgrave, M. Head-Gordon, *Acc. Chem. Res.* **2013**, *46*, 1339.
[18] J. C. Johnson, A. J. Nozik, J. Michl, *Acc. Chem. Res.* **2013**, *46*, 1290.
[19] X. Feng, A. V. Luzanov, A. I. Krylov, *J. Phys. Chem. Lett.* **2013**, *4*, 3845.
[20] S. M. Parker, T. Seideman, M. A. Ratner, T. Shiozaki, *J. Phys. Chem. C* **2014**, *118*, 12700.
[21] G. B. Piland, J. J. Burdett, R. J. Dillon, C. J. Bardeen, *J. Phys. Chem. Lett.* **2014**, *5*, 2312.
[22] W. L. Chan, M. Ligges, A. Jailaubekov, L. Kaake, L. Miaja-Avila, X. Y. Zhu, *Science* **2011**, *334*, 1541.
[23] S. Lukman, K. Chen, J. M. Hodgkiss, D. H. P. Turban, N. D. M. Hine, S. Dong, J. Wu, N. C. Greenham, A. J. Musser, *Nat. Commun.* **2016**, *7*, 13622.
[24] S. Lukman, A. J. Musser, K. Chen, S. Athanasopoulos, C. K. Yong, Z. Zeng, Q. Ye, C. Chi, J. M. Hodgkiss, J. Wu, R. H. Friend, N. C. Greenham, *Adv. Funct. Mater.* **2015**, *25*, 5452.
[25] M. Chen, Y. J. Bae, C. M. Mauck, A. Mandal, R. M. Young, M. R. Wasielewski, *J. Am. Chem. Soc.* **2018**, *140*, 9184.
[26] C. Mauck, K. Brown, N. Horwitz, M. R. Wasielewski, *J. Phys. Chem. A* **2015**, *119*, 5587.
[27] J. C. Johnson, A. Akdag, M. Zamadar, X. Chen, A. F. Schwerin, I. Paci, M. B. Smith, Z. Havlas, J. R. Miller, M. A. Ratner, A. J. Nozik, J. Michl, *J. Phys. Chem. B* **2013**, *117*, 4680.
[28] J. Zirzlmeier, R. Casillas, S. R. Reddy, P. B. Coto, D. Lehnherr, E. T. Chernick, I. Papadopoulos, M. Thoss, R. R. Tykwinski, D. M. Guldi, *Nanoscale* **2016**, *8*, 10113.
[29] I. Papadopoulos, J. Zirzlmeier, C. Hetzer, Y. J. Bae, M. D. Krzyaniak, M. R. Wasielewski, T. Clark, R. R. Tykwinski, D. M. Guldi, *J. Am. Chem. Soc.* **2019**, *141*, 6191.
[30] B. S. Basel, R. M. Young, M. D. Krzyaniak, I. Papadopoulos, C. Hetzer, Y. Gao, N. T. La Porte, B. T. Phelan, T. Clark, R. R. Tykwinski, M. R. Wasielewski, D. M. Guldi, *Chem. Sci.* **2019**, *10*, 11130.
[31] J. Zirzlmeier, D. Lehnherr, P. B. Coto, E. T. Chernick, R. Casillas, B. S. Basel, M. Thoss, R. R. Tykwinski, D. M. Guldi, *Proc. Natl. Acad. Sci. U. S. A.* **2015**, *112*, 5325.
[32] B. S. Basel, J. Zirzlmeier, C. Hetzer, B. T. Phelan, M. D. Krzyaniak, S. R. Reddy, P. B. Coto, N. E. Horwitz, R. M. Young, F. J. White, F. Hampel, T. Clark, M. Thoss, R. R. Tykwinski, M. R. Wasielewski, D. M. Guldi, *Nat. Commun.* **2017**, *8*, 15171.
[33] E. Kumarasamy, S. N. Sanders, M. J. Y. Tayebjee, A. Asadpoordarvish, T. J. H. Hele, E. G. Fuemmeler, A. B. Pun, L. M. Yablon, J. Z. Low, D. W. Paley, J. C. Dean, B. Choi, G. D. Scholes, M. L. Steigerwald, N. Ananth, D. R. McCamey, M. Y. Sfeir, L. M. Campos, *J. Am. Chem. Soc.* **2017**, *139*, 12488.
[34] S. N. Sanders, E. Kumarasamy, A. B. Pun, M. T. Trinh, B. Choi, J. Xia, E. J. Taffet, J. Z. Low, J. R. Miller, X. Roy, X.-Y. Zhu, M. L. Steigerwald, M. Y. Sfeir, L. M. Campos, *J. Am. Chem. Soc.* **2015**, *137*, 8965.
[35] S. N. Sanders, E. Kumarasamy, A. B. Pun, M. L. Steigerwald, M. Y. Sfeir, L. M. Campos, *Chem* **2016**, *1*, 505.
[36] S. W. Eaton, L. E. Shoer, S. D. Karlen, S. M. Dyar, E. A. Margulies, B. S. Veldkamp, C. Ramanan, D. A. Hartzler, S. Savikhin, T. J. Marks, M. R. Wasielewski, *J. Am. Chem. Soc.* **2013**, *135*, 14701.
[37] K. Nagarajan, A. R. Mallia, V. S. Reddy, M. Hariharan, *J. Phys. Chem. C* **2016**, *120*, 8443.
[38] A. K. Le, J. A. Bender, S. T. Roberts, *J. Phys. Chem. Lett.* **2016**, *7*, 4922.
[39] Y. V. Aulin, K. M. Felter, D. D. Günbas, R. K. Dubey, W. F. Jager, F. C. Grozema, *ChemPlusChem* **2018**, *83*, 230.
[40] A. K. Le, J. A. Bender, D. H. Arias, D. E. Cotton, J. C. Johnson, S. T. Roberts, *J. Am. Chem. Soc.* **2018**, *140*, 814.
[41] C. Schierl, A. Niazov-Elkan, L. J. W. Shimon, Y. Feldman, B. Rybtchinski, D. M. Guldi, *Nanoscale* **2018**, *10*, 20147.
[42] K. M. Lefler, K. E. Brown, W. A. Salamant, S. M. Dyar, K. E. Knowles, M. R. Wasielewski, *J. Phys. Chem. A* **2013**, *117*, 10333.
[43] E. A. Margulies, J. L. Logsdon, C. E. Miller, L. Ma, E. Simonoff, R. M. Young, G. C. Schatz, M. R. Wasielewski, *J. Am. Chem. Soc.* **2017**, *139*, 663.

[44] S. W. Eaton, S. A. Miller, E. A. Margulies, L. E. Shoer, R. D. Schaller, M. R. Wasielewski, *J. Phys. Chem. A* **2015**, *119*, 4151.
[45] P. E. Hartnett, E. A. Margulies, C. M. Mauck, S. A. Miller, Y. Wu, Y.-L. Wu, T. J. Marks, M. R. Wasielewski, *J. Phys. Chem. B* **2016**, *120*, 1357.
[46] C. M. Mauck, P. E. Hartnett, E. A. Margulies, L. Ma, C. E. Miller, G. C. Schatz, T. J. Marks, M. R. Wasielewski, *J. Am. Chem. Soc.* **2016**, *138*, 11749.
[47] C. E. Miller, M. R. Wasielewski, G. C. Schatz, *J. Phys. Chem. C* **2017**, *121*, 10345.
[48] T. Mukhopadhyay, A. J. Musser, B. Puttaraju, J. Dhar, R. H. Friend, S. Patil, *J. Phys. Chem. Lett.* **2017**, *8*, 984.
[49] C. M. Mauck, P. E. Hartnett, Y. L. Wu, C. E. Miller, T. J. Marks, M. R. Wasielewski, *Chem. Mater.* **2017**, *29*, 6810.
[50] C. M. Mauck, Y. J. Bae, M. Chen, N. Powers-Riggs, Y.-L. Wu, M. R. Wasielewski, *ChemPhotoChem* **2018**, *2*, 223.
[51] L. Shen, Z. Tang, X. Wang, H. Liu, Y. Chen, X. Li, *Phys. Chem. Chem. Phys.* **2018**, *20*, 22997.
[52] M. Grzybowski, D. T. Gryko, *Adv. Opt. Mater.* **2015**, *3*, 280.
[53] D. Chandran, K.-S. Lee, *Macromol. Res.* **2013**, *21*, 272.
[54] H. Langhals, T. Potrawa, H. Nöth, G. Linti, *Angew. Chem., Int. Ed.* **1989**, *28*, 478.
[55] H. Bürckstümmer, A. Weissenstein, D. Bialas, F. Würthner, *J. Org. Chem.* **2011**, *76*, 2426.
[56] J. Dhar, D. P. Karothu, S. Patil, *Chem. Commun.* **2015**, *51*, 97.
[57] J. Calvo-Castro, M. Warzecha, A. R. Kennedy, C. J. McHugh, A. J. McLean, *Cryst. Growth Des.* **2014**, *14*, 4849.
[58] M. A. Naik, S. Patil, *J. Polym. Sci., Part A: Polym. Chem.* **2013**, *51*, 4241.
[59] B. Tieke, A. R. Rabindranath, K. Zhang, Y. Zhu, *Beilstein J. Org. Chem.* **2010**, *6*, 830.
[60] S. Qu, H. Tian, *Chem. Commun.* **2012**, *48*, 3039.
[61] C. B. Nielsen, M. Turbiez, I. McCulloch, *Adv. Mater.* **2013**, *25*, 1859.
[62] Y. Li, P. Sonar, L. Murphy, W. Hong, *Energy Environ. Sci.* **2013**, *6*, 1684.
[63] M. Kaur, D. H. Choi, *Chem. Soc. Rev.* **2015**, *44*, 58.
[64] S. Loser, C. J. Bruns, H. Miyauchi, R. P. Ortiz, A. Facchetti, S. I. Stupp, T. J. Marks, *J. Am. Chem. Soc.* **2011**, *133*, 8142.
[65] A. Tang, C. Zhan, J. Yao, E. Zhou, *Adv. Mater.* **2017**, *29*, 1600013.
[66] Y. Geng, A. Tang, K. Tajima, Q. Zeng, E. Zhou, *J. Mater. Chem. A* **2019**, *7*, 64.
[67] S. Masoomi-Godarzi, M. Liu, Y. Tachibana, L. Goerigk, K. P. Ghiggino, T. A. Smith, D. J. Jones, *Adv. Energy Mater.* **2018**, *8*, 1801720.
[68] D. Sahu, C.-H. Tsai, H.-Y. Wei, K.-C. Ho, F.-C. Chang, C.-W. Chu, *J. Mater. Chem.* **2012**, *22*, 7945.
[69] J. Yang, F. Zhu, W. Chen, B. Li, L. Zhang, R. Xie, *J. Chem. Res.* **2005**, *2005*, 184.
[70] E. Zhou, S. Yamakawa, K. Tajima, C. Yang, K. Hashimoto, *Chem. Mater.* **2009**, *21*, 4055.
[71] A. T. Yiu, P. M. Beaujuge, O. P. Lee, C. H. Woo, M. F. Toney, J. M. J. Fréchet, *J. Am. Chem. Soc.* **2012**, *134*, 2180.
[72] S.-Y. Liu, D.-G. Wang, A.-G. Zhong, H.-R. Wen, *Org. Chem. Front.* **2018**, *5*, 653.
[73] S. Grimme, J. Antony, S. Ehrlich, H. Krieg, *J. Chem. Phys.* **2010**, *132*, 154104.
[74] S. Grimme, S. Ehrlich, L. Goerigk, *J. Comput. Chem.* **2011**, *32*, 1456.
[75] H. Kruse, S. Grimme, *J. Chem. Phys.* **2012**, *136*, 154101.
[76] L. Goerigk, N. Mehta, *Aust. J. Chem.* **2019**, *72*, 563.
[77] F. Jensen, *Wiley Interdiscip. Rev.: Comput. Mol. Sci.* **2013**, *3*, 273.
[78] R. Ditchfield, W. J. Hehre, J. A. Pople, *J. Chem. Phys.* **1971**, *54*, 724.
[79] K. C. Krishnapriya, P. Roy, B. Puttaraju, U. Salzner, A. J. Musser, M. Jain, J. Dasgupta, S. Patil, *Nat. Commun.* **2019**, *10*, 33.
[80] A solvent change to benzonitrile did not lead to any significant differences (Figure S1, Supporting Information).
[81] N. J. Hestand, F. C. Spano, *Chem. Rev.* **2018**, *118*, 7069.
[82] E. A. Margulies, L. E. Shoer, S. W. Eaton, M. R. Wasielewski, *Phys. Chem. Chem. Phys.* **2014**, *16*, 23735.
[83] H. Yamagata, C. M. Pochas, F. C. Spano, *J. Phys. Chem. B* **2012**, *116*, 14494.
[84] J. P. Mora-Fuentes, I. Papadopoulos, D. Thiel, R. Álvarez-Boto, D. Cortizo-Lacalle, T. Clark, M. Melle-Franco, D. M. Guldi, A. Mateo-Alonso, *Angew. Chem., Int. Ed.* **2020**, *59*, 1113.
[85] N. V. Korovina, J. Joy, X. Feng, C. Feltenberger, A. I. Krylov, S. E. Bradforth, M. E. Thompson, *J. Am. Chem. Soc.* **2018**, *140*, 10179.
[86] Please note that the time resolution of our setup of 200 ps hampers accuracy in some cases.
[87] B. S. Basel, J. Zirzlmeier, C. Hetzer, S. R. Reddy, B. T. Phelan, M. D. Krzyaniak, M. K. Volland, P. B. Coto, R. M. Young, T. Clark, M. Thoss, R. R. Tykwinski, M. R. Wasielewski, D. M. Guldi, *Chem* **2018**, *4*, 1092.
[88] E. A. Margulies, C. E. Miller, Y. Wu, L. Ma, G. C. Schatz, R. M. Young, M. R. Wasielewski, *Nat. Chem.* **2016**, *8*, 1120.
[89] (T_1 + T_1) formation of less than 100 ns hampers any meaningful investigations based on time-resolved EPR.